Cu–Cu bonding using bimodal submicron–nano Cu paste and its application in die attachment for power device

Yu-bo Xiao[1,2], Yue Gao[2], Zhi-Quan Liu[2,3,*] ⓘD, Rong Sun[2,3], and Yang Liu[1,*]

[1] *School of Material Science and Engineering, Harbin University of Science and Technology, Harbin 150040, China*

[2] *Shenzhen Institute of Advanced Electronic Materials, Shenzhen Institute of Advanced Technology, Chinese Academy of Sciences, Shenzhen 518055, China*

[3] *Shenzhen College of Advanced Technology, University of Chinese Academy of Sciences, Shenzhen 518055, China*

ABSTRACT

The bimodal submicron–nano Cu paste was developed for the application in die attachment for power device, and robust Cu sinter joints could be realized at a low pressure of 0.4 MPa in N_2 atmosphere. The ratio of submicron-Cu and nano-Cu particles had a great influence on the bonding performance of Cu paste. The optimized content ratio of submicron-Cu and nano-Cu particles was 1:1, with which the high shear strength of 40 MPa could be achieved at 250 °C, and an ultra-high shear strength of 60.4 MPa could be reached at 300 °C. At the same time, the porosity of the sintered body could be reduced to 11.3%, while the resistivity could be reduced to 11.2 μΩ cm. Compared with the Cu sinter joint of pure nano-Cu paste at 300 °C, the shear strength of submicron:nano = 1:1 Cu paste was increased by 27.3 MPa, the porosity was reduced to 33.7%, and the resistivity was reduced to 16.7%. And the reasons for this phenomenon are explained from the packing density of the Cu particles, the size, and proportion of the Cu particles. The presented bimodal Cu paste possessed high bonding performance which had enormous potential in industrial production.

1 Introduction

With the development of electronic devices in the direction of miniaturization, high power density, and high integration, the operating temperature of the power devices was expected to raise to 250 °C [1, 2]. The wide band-gap (WBG) semiconductors represented by GaN and SiC possessed advantages such as high output power, high operating frequency, high thermal conductivity, and high thermal reliability [3–6], which ensured their usage in electric vehicles, aerospace, and other fields at harsh environments. To meet the requirement of such harsh working environment, novel packaging materials

should be developed because traditional materials, such as Sn-based bonding materials, could not provide reliable package. The die-attachment packaging of Sn-based solder became unreliable under high temperature, frequent thermal shock, and fatigue caused by relative internal stress. Therefore, it is urgent to seek a high-reliability package material with excellent thermal reliability for WBG semiconductor packaging.

Sinterable metallic particle paste was widely studied and was regarded as a high-reliability die-attach material. The Ag nanoparticle paste, possessing advantages such as low sintering temperature, high re-melting temperature, and excellent thermal conductivity, has become an attractive candidate for the high thermal reliable die-attach material [7–10]. However, electro-chemical migration of Ag and its high price limited its industrial application. In contrast, Cu nanoparticle paste attracted attention in recent because of its low price, preferable electrical/thermal conductivity, and good electromigration resistance [11]. However, the serious oxidation problem limited the application of Cu nanoparticle paste. When oxidation occurred, the Cu oxide layer covered on the Cu particles greatly hinders the sintering process. Therefore, the sintering of Cu nanoparticle paste often required high temperature (> 350 °C) [12, 13], reductive gas protection [14, 15], or high pressure (> 5 MPa) assistance to overcome the oxidation [16–18]. Among them, the higher temperature is conducive to the in-situ formation of nano-Cu from CuO to combine with larger Cu fillers [19]. Moreover, considering the complex fabrication of the Cu nanoparticles, the Cu paste completely composed by nano-Cu could erase its price advantage. The price of submicron-Cu particles is low, and the specific surface area of submicron-Cu particles is smaller than that of nano-Cu particles for the same volume, and the agglomeration phenomenon is relatively insignificant. At the same time, the mixture of submicron-Cu and nano-Cu makes that the nano-Cu fills the gaps of the submicron-Cu, resulting in a denser sintered structure. Therefore, it is possible to consider mixing submicron-Cu and nano-Cu to prepare die-attach paste for power device package [20]. Moreover, in engineering applications, particles with different size specifications are often mixed in a certain ratio to achieve a higher density of paste [21, 22]. Therefore, the use of a mixture of nano-Cu particles and submicron-Cu particles to prepare a paste is

expected to further improve the conductivity of the sintered body on the basis of reducing costs and achieving higher densification and reduction of sintering shrinkage.

Herein, we developed a novel low-pressure sinterable bimodal Cu paste by mixing nano-Cu particles (solvothermal synthesis) and submicron-Cu particles (commercially available), which could form ultra-high-strength Cu–Cu joints under moderate sintering conditions. For the previous sintering research of bimodal Cu paste, most of them were carried out under high pressure or reductive atmosphere [15, 17], but our bimodal Cu paste can not only solve the problem of difficult sintering of submicron-Cu particles at low temperature and low pressure, but also the addition of nano-Cu particles can be used as a bridge to assist the sintering of submicron-Cu, and at the same time, the sintering is carried out in a non-reductive N_2 atmosphere, and the Cu is almost not oxidized. Compared with the sintering of nano-Cu particle paste, the Cu sinter joint of the bimodal Cu paste had a higher bonding strength (40 MPa) at a reduced sintering temperature (250 °C). At the same time, it was better than nano-Cu particle paste in terms of conductivity and porosity, ensuring its potential in industrial applications.

2 Experimental procedure

2.1 Preparation of submicron–nano Cu composite paste

Initially, copper hydroxide (1.54 mol/L) was completely dissolved in a mixed solution of isopropanolamine (5 mL) and triethylene glycol (5 mL), and the Cu^{2+} complex was formed under magnetic stirring at 60 °C. Then the Cu^{2+} complex was added to 40 ml of ethylene glycol solution containing sodium hypophosphite (3.14 mol/L), reacted for 10 min at 60 °C, and then Cu submicron particles with a particle size of about 1 μm were added into the resulting solution and continued to stir. The submicron–nano Cu composite particles were centrifuged at 8000 rpm for 10 min to obtain a composite paste with high Cu content. In order to optimize the performance of Cu-sintered joints, the mass ratio of submicron/nanoparticles was designed to be 1:3; 1:1; and 3:1. For the convenience of description, Cu paste

was described as nano-Cu paste, 1:3 Cu paste, 1:1 Cu paste, and 3:1 Cu paste, corresponding to pure nanoparticle Cu paste, and the mass ratio of submicron/nanoparticles at 1:3, 1:1, and 3:1 Cu paste.

2.2 Fabrication of Cu–Cu joints

The polished bare Cu substrates ($12 \times 12 \times 1$ mm^3) and Cu dummy chip ($4 \times 4 \times 1$ mm^3) were cleaned with absolute ethanol to remove surface oxides and impurities. Then, the prepared Cu paste was printed on the Cu substrate through a stainless steel mask of 4 mm × 4 mm × 0.1 mm, and the Cu dummy chip was placed on the printed paste to produce a sandwich structure sample. The prepared samples were sintered at 200 °C, 250 °C, and 300 °C for 30 min in an N$_2$ atmosphere with a pressure of 0.4 MPa, and the heating rate was controlled to 15 °C/min.

2.3 Characterization and measurement

The formed sandwich joints were tested for shear strength (DAGE 4000, Dage; shear height:100 μm, shear rate:1 mm/min). The fracture structure and cross-sectional structure of the sintered Cu joint were observed by scanning electron submicronscope (SEM, FEI Nova Nano SEM 450). The cross-section samples were made by ion milling and polishing processes. The thickness, length, and width of the die-attach layer were measured by the step meter (DektakXT), and sheet resistivity (R) of the die-attach layer was measured by Four-point probe (Loresta-GX Model MCP-T700). The resistivity (ρ) of the die-attach layer was calculated as follows:

$$\rho = Rhd/L, \tag{1}$$

where R is the sheet resistivity of the chip-attach layer, h, l, and d correspond to the thickness, length, and width of the die-attach layer, respectively. In addition, calculation method of porosity was based on the area of hole and Cu matrix in cross-section SEM image. The pores area was extracted from the picture (Spores), and the porosity (p) of the section was defined as follows:

$$p = S_{pores}/S_{total}, \tag{2}$$

where S_{pores} is the pore area extracted from the picture, and S_{total} is the total area of the Cu matrix.

3 Experimental results

3.1 Effects of different proportions of Cu particles on shear strength and fracture of Cu sinter joints

Figure 1 shows SEM images of Cu particles with different submicron–nano ratios. The image of pure nano-Cu particles is shown in Fig. 1a. Nano-Cu particles were spherical, the diameter of the nano-Cu particles was about 50 nm, and some of the particles were larger in size, which were caused by the agglomeration of particles during the sample preparation process. When 25 wt% submicron-Cu particles were added (Fig. 1b), some spherical particles with a diameter of about 0.5 μm could be seen. As the content of submicron-Cu particles increased, the agglomeration phenomenon gradually decreased. When the particle size was pure submicron (Fig. 1e), there was almost no agglomeration phenomenon. From Fig. 1, it could be determined that the particle size of nano-Cu was about 50 nm, and the particle size of submicron-Cu was about 0.5 μm.

Figure 2 shows the shear strength of Cu joints sintered from Cu pastes contained different ratios of submicron-Cu/nano-Cu particles. The addition of submicron-Cu caused an obvious increase in the shear strength of the sintered joints. Comparing with the shear strength of Cu-sintered joints made of pure nano-Cu paste, the bimodal Cu paste exhibited higher shear strength. The difference in shear strength was small at the sintering temperature of 200 °C, and there was a significant difference at the sintering temperature of 250 °C and 300 °C. The nano-Cu paste showed the shear strength of only 12.7 MPa at 250 °C; however, the bimodal Cu paste possessed higher shear strength. Especially, the 1:1 Cu paste possessed a highest average shear strength of 40 MPa at 250 °C. After raise the sintering temperature to 300 °C, the shear strength could further increase to 60.4 MPa at the ratio of 1:1. On the other hand, the shear strengths of nano-Cu paste at 250 °C and 300 °C were only 12.7 MPa and 40 MPa, respectively, indicating that the addition of submicron-Cu to form bimodal paste could greatly improve the Cu paste bonding ability. However, when the content of submicron-Cu decreased to 25 wt% or increased to 75 wt%, the shear strength of the sintered Cu joint decreased. Therefore, the optimized
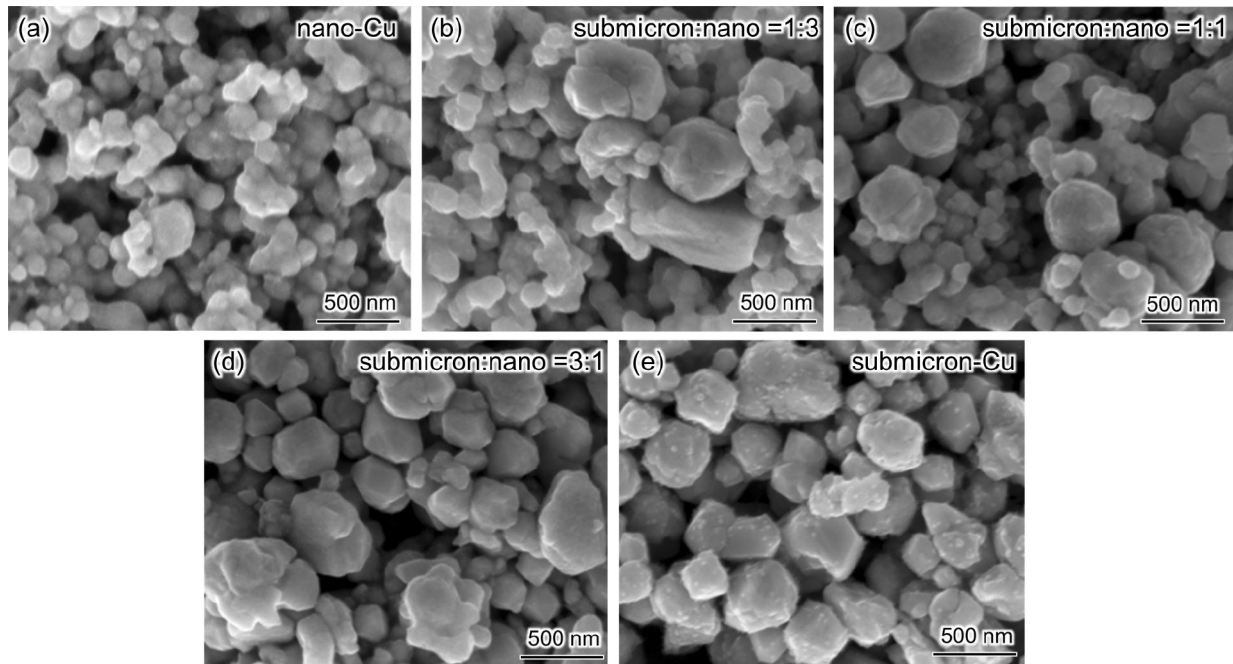
Fig. 1 The SEM observation of nano-Cu particle (**a**), submicron:nanoparticle = 1:3 (**b**), submicron:nanoparticle = 1:1 (**c**), submicron:nanoparticle = 1:3 (**d**) and submicron-Cu particle (**e**)
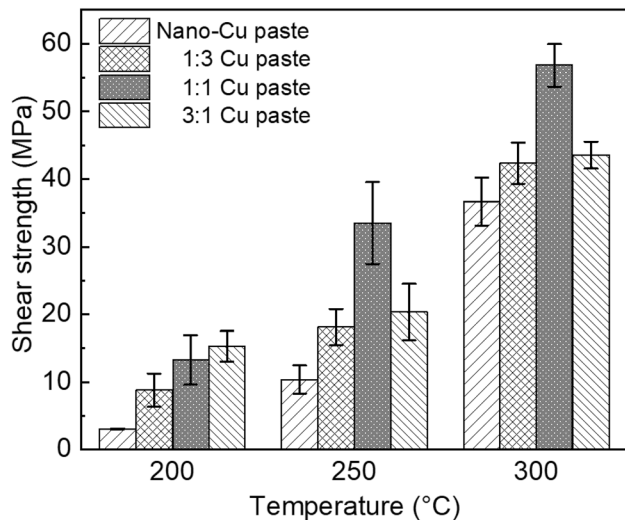

Fig. 2 The shear strength of Cu–Cu joints sintered with different kinds of Cu pastes at 200 °C, 250 °C, and 300 °C, 0.4 MPa in non-reductive N_2 atmosphere

ratio of submicron-Cu and nano-Cu was 1:1 considering the shear strength of sintered joints.

The fracture of Cu sinter joints with various bimodal Cu pastes with different ratios of submicron-Cu and nano-Cu paste was observed by SEM. Figure 3 shows the fracture surface images of Cu pastes with different proportions at a sintering temperature of 200 °C. Almost all Cu particles remained isolated

and original shapes. Only weak neck growth between adjacent particles is observed in Fig. 3. It showed that at this temperature of 200 °C, neither the bimodal Cu paste nor the nano-Cu paste had a tendency to sinter.

When the sintering temperature reached 250 °C, the fracture surface images of different proportions of Cu paste are shown in Fig. 4, in which the sintered fracture surface of nano-Cu paste, 1:3 Cu paste, and 3:1 Cu paste were compared with each other. There was not much difference in sintering at 250 °C. However, the 1:1 Cu paste had obvious changes. A large number of sintered necks could be seen on the fracture surface, corresponding to the obvious increase in shear strength in Fig. 2. But some small particles could still be seen isolated, and no sintered structure was formed (Fig. 4c). It showed that 1:1 Cu paste had a preferential sintering trend compared with other Cu pastes.

The fracture surface images of Cu pastes with different proportions at a sintering temperature of 300 °C are illustrated in Fig. 5. At a sintering temperature of 300 °C, almost all Cu pastes could form a denser structure. But compared with sintered nano-Cu paste (Fig. 5a), bimodal Cu paste had a dense-sintered structure. When the proportion of submicron-Cu was increased to 25 wt% (1:3 Cu paste), the dimples caused by the shear test could be seen more
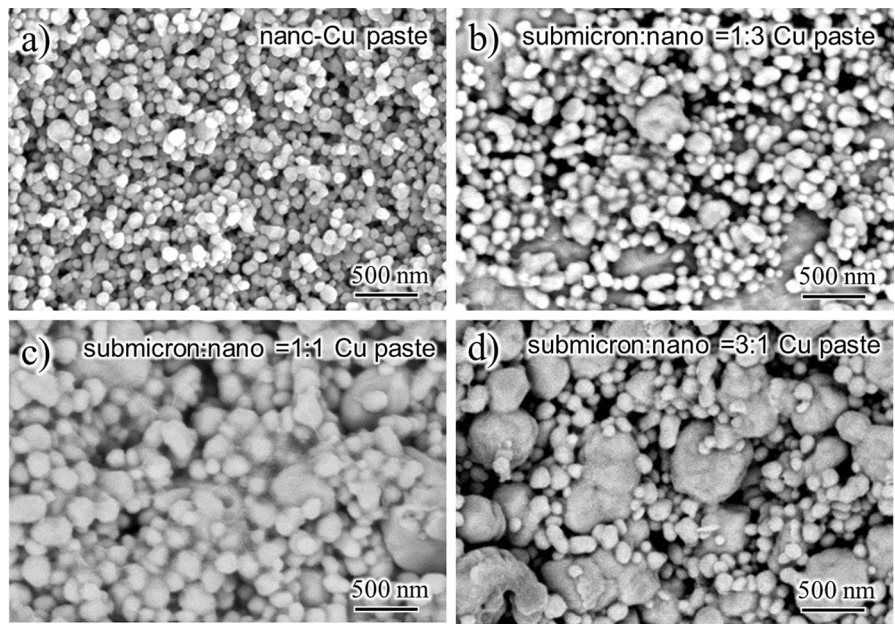
Fig. 3 SEM observations on fracture surfaces of sintered Cu joints by using nano-Cu paste (**a**), submicron:nano = 1:3 Cu paste (**b**), submicron:nano = 1:1 Cu paste (**c**), and submicron:nano = 1:3 Cu paste (**d**) at 200 °C
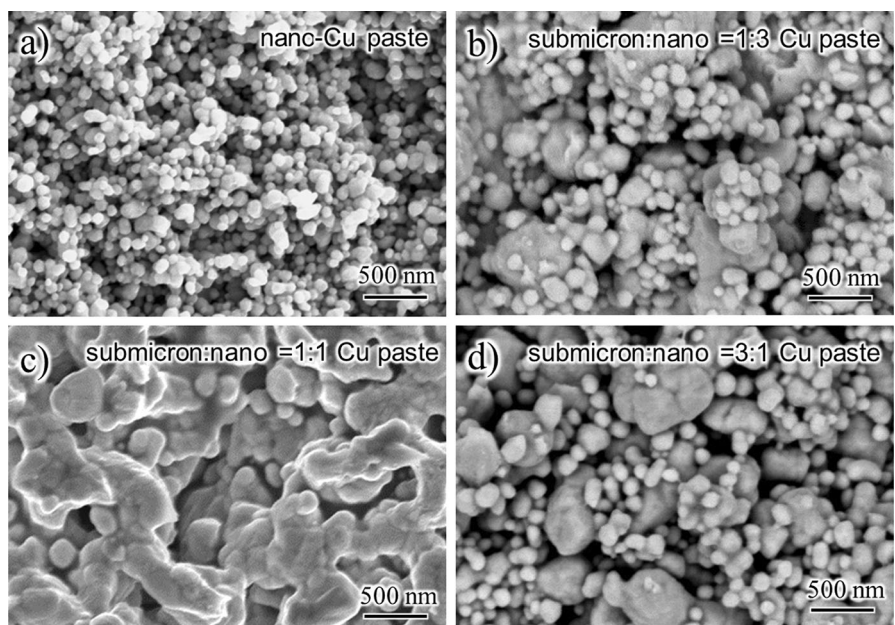

Fig. 4 SEM observations on fracture surfaces of sintered Cu joints by using nano-Cu paste (**a**), submicron:nano = 1:3 Cu paste (**b**), submicron:nano = 1:1 Cu paste (**c**), and submicron:nano = 1:3 Cu paste (**d**) at 250 °C


obviously during the shearing process (Fig. 5b). When the proportion of submicron-Cu increased to 50 wt% (1:1 Cu paste), the sintering compactness reached the best state (Fig. 5c). When the ratio of submicron-Cu was increased to 75 wt% (3:1 paste), the compactness of sintering decreased, and the presence of some single Cu particles was observed (Fig. 5d). These results confirmed that the Cu paste had excellent sinterability through the addition of submicron-Cu, and robust Cu–Cu bonding could be achieved at a relative low-temperature sintering

process with low assisting pressure and without the protection of reductive gas.

3.2 Effects of different proportions of Cu particles on sintered microstructure and properties

In order to analyze the difference of sintering more clearly, we focused on the low-magnification fracture surface SEM images of 1:1 Cu paste with the highest shear strength and the pure nano-Cu paste. The

Fig. 5 SEM observations on fracture surfaces of sintered Cu joints by using nano-Cu paste (**a**), submicron:nano = 1:3 Cu paste (**b**), submicron:nano = 1:1 Cu paste (**c**), and submicron:nano = 1:3 Cu paste (**d**) at 300 °C
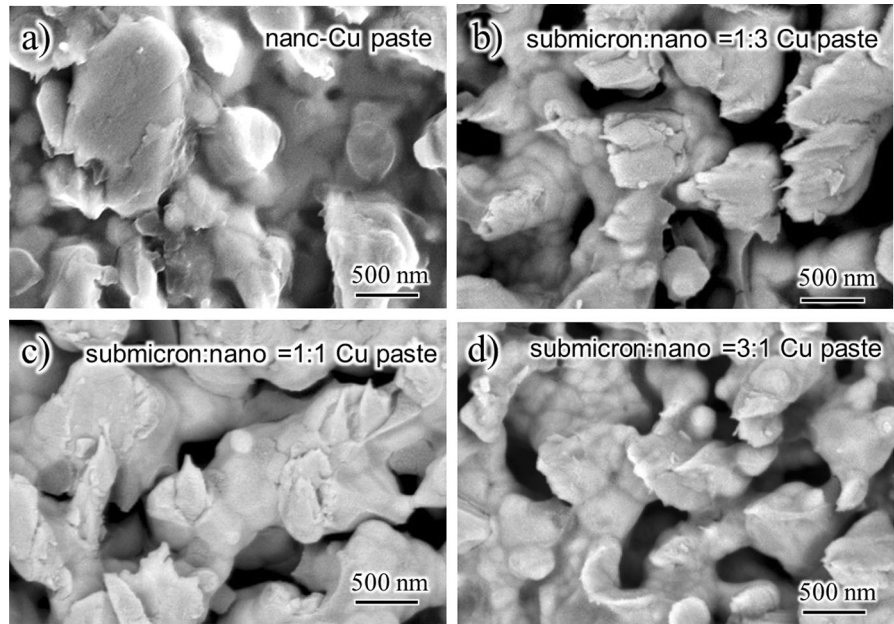
results are shown in Fig. 6. It could be seen that there were obvious cracks in the sintered section of the nano-Cu paste. This phenomenon was greatly avoided after adding submicron-Cu. The cracks were almost invisible, and the sintered structure was denser. The appearance of sintering cracks greatly affected the properties of the sintered structure. The cracks almost disappeared after the addition of submicron-Cu, which corresponded to the substantial increase in shear strength after the addition of submicron-Cu.

The cross-sectional observations of Cu joints obtained at 300 °C with nano-Cu paste and submicron-Cu-added bimodal pastes are shown in Fig. 7. When the nano-Cu paste was sintered at 300 °C, the sintering structure with obvious neck growth could

be observed. However, plenty of nano-Cu particles still remained isolate as shown in Fig. 7a. When the ratio of submicron-Cu reached 25 wt% (Fig. 7b), the isolate nano-Cu particles were relatively reduced. When the ratio of submicron-Cu reached 50 wt%, the single nano-Cu particles were almost invisible (Fig. 7c), which were much lower than that of nano-Cu paste. At the same time, the density of the sintered structure increased significantly. However, when the submicron-Cu content reached 75 wt%, some single nano-Cu particles appeared again (Fig. 7d). The results of the sintering cross section also confirmed that the proper addition of submicron-Cu could promote sintering, which was also reported in other literatures [10, 23–26].
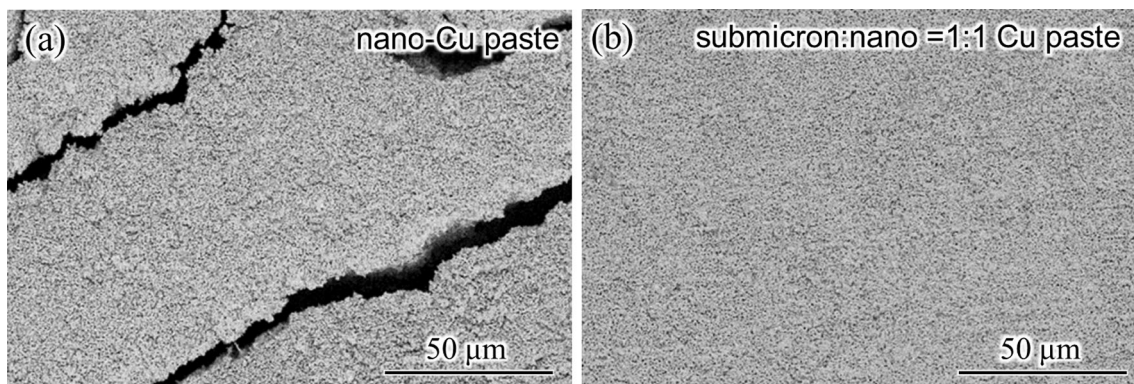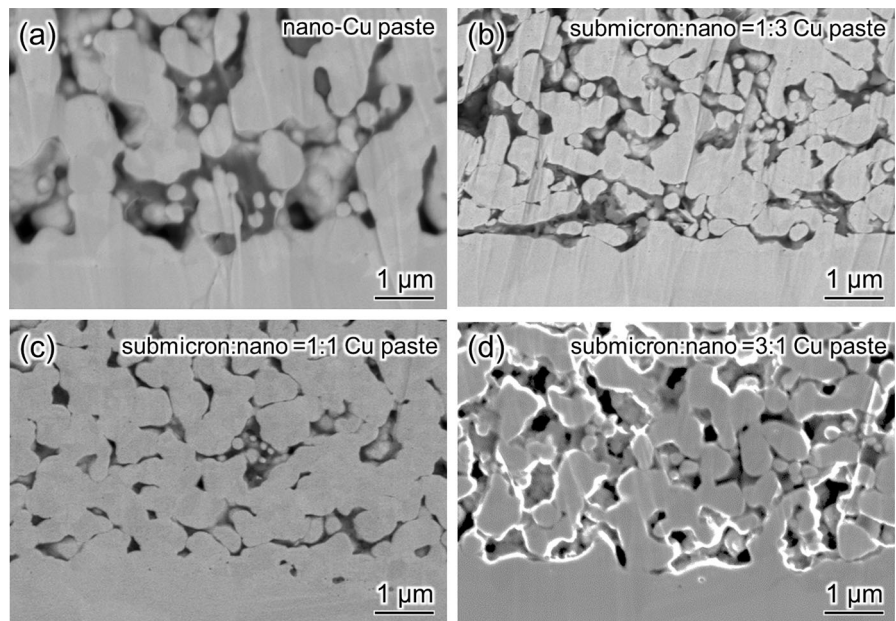

Fig. 6 SEM low-magnification observations on fracture surfaces of sintered Cu joints by using nano-Cu paste (**a**) submicron:nano = 1:1 Cu paste (**b**) at 300 °C

Fig. 7 SEM observations on crosssection of sintered Cu joints by using nano-Cu paste (**a**), submicron:nano = 1:3 Cu paste (**b**), submicron:nano = 1:1 Cu paste (**c**), and submicron:nano = 1:3 Cu paste (**d**) at 300 °C

The resistivity and porosity of the sintered layer were measured, as shown in Fig. 8. The initial resistivity and porosity of the pure nano-Cu paste were 67 μΩ cm and 34%, respectively. With the addition of submicron-Cu content from 0 to 25 wt%, the resistivity of the sintered layer decreased from 67 to 52 μΩ cm, while the porosity of the sintered layer also decreased from 34 to 30%. When the ratio of submicron-Cu reached 50 wt%, the resistivity decreased to 11.2 μΩ cm and the porosity decreased to 11.5%, which corresponded to the maximum shear strength in Fig. 2. When the content of submicron-Cu increased to 75%, the resistivity and porosity began to

increase again, reaching 53.8 μΩ cm and 24.2%, respectively. At the same time, it was accompanied by a decrease in shear strength in Fig. 2. Therefore, the porosity was directly proportional to the resistivity. The proper ratio of submicron-Cu and nano-Cu helped increase the sintered density, thereby showing low resistivity and porosity. To conclude, 1:1 Cu paste was the best in terms of shear strength and conductivity, as illustrated in Figs. 2 and 8.

4 Discussion

Through the above analysis, we could conclude that under the same process conditions, there were two main factors that affected the sintering performance of Cu particles: (1) the packing density of the particles and (2) the size and ratio of the particles. Compared with the sintering of nano-Cu particles, the addition of submicron-Cu particles could greatly increase maximum fractional packing density (PF_{MAX}) of the particles, The maximum fractional packing density (PF_{MAX}) of the spherical nanoparticles with different sizes was given by the random packing model proposed by Furnas and coworkers [27–29]. PF_{MAX} could be calculated by the following equation:

$$PF_{MAX} = PF_L + (1 - PF_L)PF_S, \tag{3}$$

where PF_L was the density of the larger particles and PF_S was the density of the smaller particles.
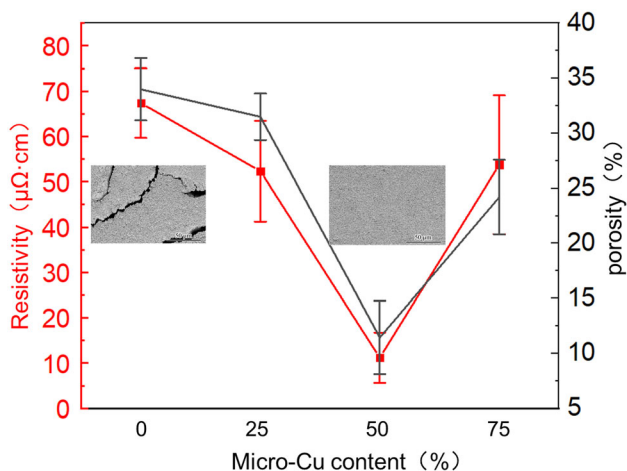

Fig. 8 Electrical resistivity and porosity of sintering layers with different composite pastes sintered at 300 °C

The fractional packing density of a monosized spherical particle system proves to be 0.65, regardless of the particle size [30]. Therefore, the density increased to 0.88 when using a bimodal submicron–nano system ($PF_L = PF_S = 0.65$). The increase in fractional packing density enhanced the bridging performance between particles and increased the density of the sintered structure, so the sintering performance of the bimodal Cu paste was significantly improved compared to the nano-Cu paste.

Compared with nano-Cu paste, the difference in packing density between Cu pastes with different ratios was not obvious. From the three ratios studied so far, the packing density of the 1:1 Cu paste should be closest to 0.88. When the packing density of the particles was not significantly different, the size and ratio of the particles become extremely important. Zuo et al. [31] mixed nano-Cu particles with a diameter of 100 nm and micron-Cu particles with a diameter of 1 μm at a mass ratio of 9:1 to develop a bimodal Cu paste. Peng et al. [23] mixed nano-Cu particles with a diameter of 10 nm and micron-Cu particles with a diameter of 1 μm in a mass ratio of 3:2, and also developed a bimodal Cu paste. It could be seen that when the size of the particles was different, the ratio between the particles also became extremely important. Under the premise of ensuring sufficient sintering, the sintering process was closely related to the decomposition of the organic layer. Therefore, TG tests were performed on 1:1 Cu paste and nano-Cu paste (with the same solvent content), respectively, and the results are shown in Fig. 9. It could be seen that as the temperature increased, the organic layer encapsulated in the Cu particles would gradually decompose. The Cu content of the 1:1 Cu paste was finally fixed at around 93%, while the Cu content of the nano-Cu paste was only around 89%, Indicating that larger submicron-Cu particles had a higher metal content because the quality of the organic layer decreased as the specific surface area of the Cu particles decreased. The lower metal content of the smaller nanoparticles resulted in many holes in the sintering layer of the nano-Cu, thereby reducing the sintering strength [32].

The sintering diagram of Cu paste with different proportions is illustrated in Fig. 10. When 25 wt% submicron-Cu was added (Fig. 10a), since the content of submicron-Cu was low, the metal content of the particles does not increase significantly while increasing the packing density. Most of the sintering
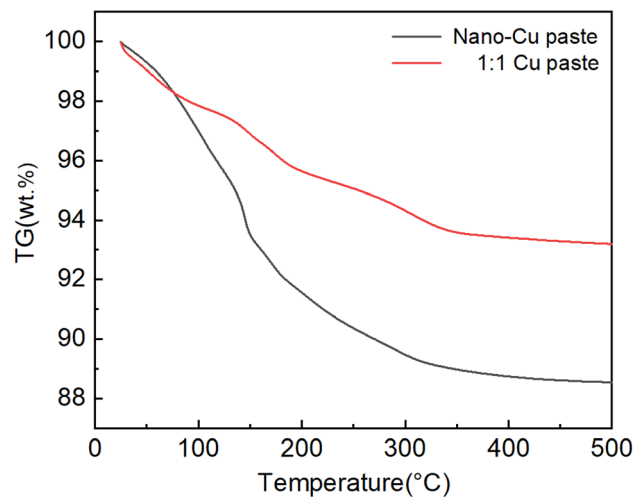

Fig. 9 TG curves for the nano-Cu paste and 1:1 Cu paste

processes were interdiffusion between nano-Cu particles, so the porosity was only slightly reduced, and the reduction in porosity was accompanied by a reduction in resistivity and an increase in strength. When 50 wt% submicron-Cu was added (Fig. 10b), the ratio of the particles reached an ideal state, and the packing density reached the maximum. During the sintering process, almost all the submicron-Cu particles were covered by nano-Cu particles. Due to the high specific surface energy of the nanoparticles, during the sintering process, the nano-Cu particles would act as a bridge to inter-diffuse the wrapped submicron-Cu particles and adjacent nano-Cu particles and finally form a dense-sintered structure. This optimal sintering state leaded to the lowest driving force required for sintering, which explained that only 1:1 Cu paste had a tendency to sinter at 250 °C. Under the combined effect of this dense-sintered structure and increased metal content, the sintered porosity was reduced to a minimum value, accompanied by a rapid decrease in resistivity and a significant increase in shear strength. The sintered structure was the densest. At the same time, the cracks in the sintering process disappeared, corresponding to the result shown in Fig. 6b. When 75 wt% submicron-Cu was added (Fig. 10c), the content of nano-Cu particles coated with micron-Cu was less due to the high content of submicron-Cu. Part of the submicron-Cu even formed an interconnection between submicron-Cu and submicron-Cu. Because of its low surface energy, the sintering of micron-Cu was mostly carried out under high temperature, high pressure, or a reductive atmosphere [33, 34]. In this
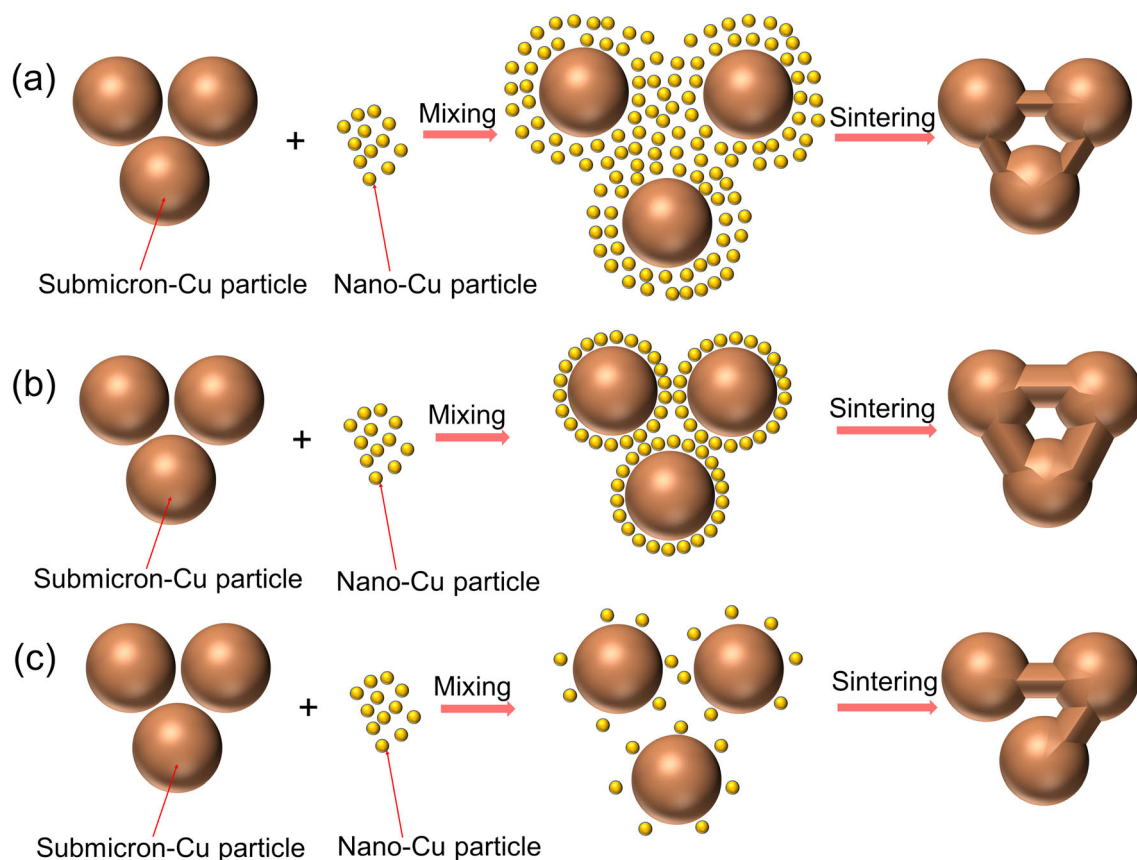
Fig. 10 Schematic diagram of submicron:nano = 1:3 Cu paste (**a**), submicron:nano = 1:1 Cu paste (**b**), submicron:nano = 3:1 Cu paste (**c**) sintered at 300 °C

study, single submicron-Cu paste was sintered at 300 °C under a pressure of 0.4 MPa, and the shear strength of Cu sinter joints was very low. It was proved that the sintering effect of single submicron-Cu was very poor under this process condition. The impact of insufficient sintering was far greater than the slight increase in the metal content, resulting in an increase in porosity and resistivity and a decrease in shear strength. In addition, the shear strength was directly related to the porosity and the resistivity of the sintered layer. Since the main fracture form of the sample was in the sintered layer, the shear strength directly corresponded to the quality of the sintered layer. Therefore, the higher the shear strength, the lower the porosity of the corresponding sintered layer, the denser the sintered structure, and the lower the resistivity of the sample.

5 Conclusion

A new bimodal submicron–nano Cu paste was successfully developed and applied to Cu–Cu bonding, which could achieve high-strength Cu sinter joints under a N_2 atmosphere and a low pressure of 0.4 MPa. This bimodal submicron–nano Cu paste not only reduced the high cost of single nano-Cu particle past but also increased the packing density of the sintered structure. At the same time, during the sintering process, the nano-Cu particles would act as a bridge to inter-diffuse the wrapped submicron-Cu particles and adjacent nano-Cu particles and finally form a dense-sintered structure. Under suitable sintering conditions (300 °C, 0.4 MPa and N_2 atmosphere), a high-strength Cu-sintered joint with shear strength of 60.4 MPa could be easily obtained from an optimized 1:1 Cu paste. At the same time, the porosity of the sintered body could be reduced to 11.3%, and the resistivity could be reduced to 11.2 µΩ cm. Compared with the Cu-sintered joint of pure

nano-Cu paste at 300 °C, the shear strength of 1:1 Cu paste was increased by 27.3 MPa, the porosity was reduced to 33.7%, and the resistivity was reduced to 16.7%. This work further extended the application of Cu paste in the packaging of high-power semiconductor devices.

Acknowledgements

Author contributions

YX is responsible for the experimental process, instrument operation, and draft preparation. YG is responsible for data analysis and article writing, Z-QL is responsible for the experimental design, guidance, and article writing, RS and YL are responsible for the technical support and discussion.

Data availability

The datasets supporting the results of this article are included within the article and its additional files.

Declarations

Conflict of interest The article does not have a conflict of interest with any other unit, institution or any individual.

References

1. H. Ji, J. Zhou, M. Liang, H. Lu, M. Li, Ultrason. Sonochem. **41**, 375 (2018)
2. Z. Liu, J. Cai, Q. Wang, Z. Wang, L. Liu, G. Zou, J. Alloys Compd. **767**, 575 (2018)
3. A.Q. Huang, in *62nd Annual IEEE International Electron Devices Meeting (IEDM)*, San Francisco, CA, 2016 Dec 03–07; (San Francisco, CA, 2016).
4. F. Roccaforte, P. Fiorenza, G. Greco, R. LoNigro, F. Giannazzo, F. Iucolano, M. Saggio, Microelectron. Eng. **187**, 66 (2018)
5. K. Shenai, IEEE Trans. Electron Devices **62**(2), 248 (2015)
6. M. Shur, Solid-State Electron. **155**, 65 (2019)
7. H. Fang, C. Wang, S. Zhou, Q. Kang, T. Wang, D. Yang, Y. Tian, J. Mater. Sci. **31**(8), 6497 (2020)
8. F. Yang, B. Hu, Y. Peng, C. Hang, H. Chen, C. Lee, J. Wei, M. Li, J. Mater. Sci. **30**(6), 5526 (2019)
9. F. Yu, R.W. Johnson, M.C. Hamilton, IEEE Trans. Comp. Packag. Manuf. Technol. **5**(9), 1258 (2015)
10. Z. Zhang, C. Chen, Y. Yang, H. Zhang, D. Kim, T. Sugahara, S. Nagao, K. Suganuma, J. Alloys Compd. **780**, 435 (2019)
11. Y. Gao, Y.B. Xiao, J. Mater. Sci. **33**, 3576 (2022)
12. Y. Kobayashi, T. Shirochi, Y. Yasuda, T. Morita, Int. J. Adhes. Adhes. **33**, 50 (2012)
13. Y. Kobayashi, Y. Abe, T. Maeda, Y. Yasuda, T. Morita, J. Mater. Res. Technol. **3**(2), 114 (2014)
14. D. Yamagiwa, T. Matsuda, H. Furusawa, K. Sato, H. Tatsumi, T. Sano, Y. Kashiba, A. Hirose, J. Mater. Sci. **32**(14), 19031 (2021)
15. Y. Zuo, S. Carter-Searjeant, M. Green, L. Mills, S. H. Mannan, Materials Letters. **276** (2020)
16. J.-W. Yoon, J.-H. Back, Materials **11**(11), 2105 (2018)
17. J. Liu, H. Chen, H. Ji, M. Li, ACS Appl. Mater. Interfaces. **8**(48), 33289 (2016)
18. T. Yamakawa, T. Takemoto, M. Shimoda, H. Nishikawa, K. Shiokawa, N. Terada, J. Electron. Mater. **42**(6), 1260 (2013)
19. T.F. Chen, K.S. Siow, J. Alloys Compd. **866**, 158783 (2021)
20. J.H. Prosser, T. Brugarolas, S. Lee, A.J. Nolte, D. Lee, Nano Lett. **12**(10), 5287 (2012)
21. R.Y. Yang, R.P. Zou, A.B. Yu, S.K. Choi, J. Colloid Interface Sci. **299**(2), 719 (2006)
22. A. Pajor-Świerzy, Y. Farraj, A. Kamyshny, S.J.C. Magdassi, S.A. Physicochemical, E. Aspects, Air stable copper-silver core-shell submicron particles: Synthesis and conductive ink formulation. Colloids Surf. A **521**, 272 (2017)
23. Y. Peng, Y. Mou, J. Liu, M. Chen, J. Mater. Sci. **31**(11), 8456 (2020)
24. S.-J. Joo, H.-J. Hwang, H.-S. Kim, Nanotechnology **25**(26), 265601 (2014)
25. J. Jiu, H. Zhang, S. Koga, S. Nagao, Y. Izumi, K. Suganuma, J. Mater. Sci.-Mater. Electron. **26**(9), 7183 (2015)
26. J.W. Oh, Y. Seong, D.S. Shin, S.J. Park, Powder Technol. **352**, 42 (2019)
27. C.C. Furnas, Ind. Eng. Chem. **23**, 1052 (1931)
28. R.M. German, Metall. Trans. A **23**(5), 1455 (1992)
29. R.M. German, M. Bulger, Int. J. Powder Metall. **28**(3), 301 (1992)
30. R.K. McGeary, J. Am. Ceram. Soc. **44**(10), 513 (1961)
31. Y. Zuo, J. Shen, J. Xie, L. Xiang, J. Mater. Process. Technol. **257**, 250 (2018)
32. Y. Morisada, T. Nagaoka, M. Fukusumi, Y. Kashiwagi, M. Yamamoto, M. Nakamoto, H. Kakiuchi, Y. Yoshida, J. Electron. Mater. **40**(12), 2398 (2011)

33. X. Liu, H. Nishikawa, Scr. Mater. **120**, 80 (2016)
34. J. Kaehler, N. Heuck, A. Wagner, A. Stranz, E. Peiner, A. Waag, IEEE Trans. Comp. Packag. Manuf. Technol. **2**(10), 1587 (2012)

Publisher's Note Springer Nature remains neutral with regard to jurisdictional claims in published maps and institutional affiliations.